Noname manuscript No.
(will be inserted by the editor)

Coordinate descent optimization for winged-UAV design

Haowei Gu · Ximin Lyu · Zexiang Li · Fu Zhang

Received: date / Accepted: date

Abstract In this paper, a powerful optimization framework is proposed to design highly efficient winged unmanned aerial vehicle (UAV) that is powered by electric motors. In the proposed approach, the design of key UAV parameters including both aerodynamic configurations, (e.g. wing span, sweep angle, chord, taper ratio, cruise speed and angle of attack) and the propulsion systems (e.g. propeller, motor and battery) are cast into an unified optimization problem, where the optimization objective is the design goal (e.g. flight range, endurance). Moreover, practical constraints are naturally incorporated into the design procedures as constraints of the optimization problem. These constraints may arise from the preliminary UAV shape and layout determined by industrial design, weight constraints, etc. The backend of the optimization based UAV design framework are highly accurate aerodynamic models and propulsion system models proposed in this paper and verified by actual experiment data. The optimization framework is inherently non-convex and involves both continuous variables (e.g. the aerodynamic configuration parameters) and discrete variables (e.g. propulsion system combinations). To solve this problem, a novel coordinate descent method is proposed. Trial designs show that the proposed method works rather efficiently, converging in a few iterations. And the returned solution is rather stable with different initial conditions. Finally,

*Research supported by Hong Kong ITF Foundation (ITS/334/15FP).

Haowei Gu
Room 2014, CYT building, HKUST, Clear Water Bay, Kowloon, Hong Kong
Tel.: +852-67607724
E-mail: hguad@connect.ust.hk

Ximin Lyu
Room 2014, CYT building, HKUST, Clear Water Bay, Kowloon, Hong Kong
Tel.: +852-65609809
E-mail: xlvaa@connect.ust.hk

Zexiang Li
Room 2014, CYT building, HKUST, Clear Water Bay, Kowloon, Hong Kong
E-mail: eezxli@ust.hk

Fu Zhang
HW7-18, University of Hong Kong, Pokfulam, Hong Kong
E-mail: fuzhang@hku.hk

the entire approach is applied to design a quadrotor tail-sitter VTOL UAV. The designed UAV is validated by both CFD simulations and intensive real-world flight tests.

Keywords Coordinate descent method · Optimization based design · UAV

1 Introduction

In recent years, research interests to unmanned aerial vehicles (UAVs) are dramatically increased, due to their great potential in various fields, such as aerial photography, parcel delivery, precise agriculture, remote sensing, etc. UAVs currently under investigation are mainly divided into two classes: winged UAVs (including monoplane, biplane, flying wing aircraft etc.) and wingless UAVs (multi rotors UAVs, helicopter and ect.), of which winged UAVs are very suitable for range demanding applications because of their higher aerodynamic efficiency, faster airspeed, longer flight range and higher effective load. To meet the increasing efficiency requirements, winged UAV design poses a grand challenge that involves many key components: aerodynamic design [1], structure design [2], propulsion system design [3], etc. In addition, the design process is usually subject to various practical constraints such as size, weight, and layout determined by industrial design. Finally, the design objective is also very diverse among different scenarios. For example, parcel delivery UAVs are expected to reach longer range with higher maximum takeoff weight (MTOW) but surveillance UAVs may prefer longer flight endurance for a fixed take-off weight.

To solve such a complex design problem involving various constrains and different design objectives, two main design approaches have been mainly used in the field. The traditional design method by human designers, especially for model airplanes, relies heavily on the designers' experience and it usually breaks into two separate design steps as shown in [4], [5] and [6]: firstly, the aerodynamic configurations are determined from the designers' past experiences and common senses on the effects of key aerodynamic configurations such as airfoil type, wingspan, aspect ratio, swept back angle, etc. And then, the proper propeller, motor and battery are determined from their respective pitch angle, motor KV and battery capacity. A drawback of this design method is that in each of these two steps, only the dominant factors are considered while secondary factors are ignored as it is difficult for human designers to exactly optimize multi-variables all at the same time. Moreover, in such a sequential procedure, the aerodynamic configuration and propulsion system are optimized separately while they are really related to each other. As a consequence, the design is usually not optimal. It is also quite difficult for human designers to consider these constraints mentioned above.

Another popular method is known as the multidisciplinary design optimization (MDO) [7], which uses optimization approaches to solve the system design problems involving varies subsystems and internal connections. In past decades, MDO has been investigated widely and applied in a number of fields. For example, Masoud *et al.* [8] applied particle swarm optimization method to optimize the multidisciplinary design of a small satellite launch vehicle; John *et al.* [9] maximized the total data downloaded of small satellite, which demonstrated the application of MDO method in large-scale engineering system problem; Turaj *et al.* [10] applied MDO in the system level design of offshore wind turbines to minimize the

levelized cost energy. Besides the MDO formulations, there are also many work on solving the formulated optimization problem. Zi *et al.* [11] used multi-objective optimization concept to simultaneously optimize the mechanism and control of hybrid-driven based cable parallel manipulators. Alessio [12] introduced an multi-objective optimization algorithm to simultaneously minimize power loss and maximize contact pressure in gear designs. For optimization problem involving single objective function, Cramer *et al.* [13] introduced an approach known as "Multidisciplinary feasible (MDF)" composed of a complete multidisciplinary design analysis (MDA) and an optimizer, which is the most common and simplest way to solve the MDO problems. To avoid the formulation of complete MDA, Balling *et al.* [14] proposed "Individual discipline feasible (IDF)" method; Braun *et al.* detailed a decentralized and decomposed bi-level optimization scheme "Collaborative optimization (CO)" in [15] to eliminate the the interdisciplinary discrepancies while satisfying the disciplinary constrains.

The MDO method have also been applied to aircraft design, which relies strongly on accurate aerodynamic model and involve immense fluid dynamics computation. Thus, the MDO is usually rather time consuming and high cost, which has mainly been used to design the commercial manned aircrafts. For example, Manning *et al.* [16] used the MDO method to design and optimize a supersonic aircraft, Peter *et al.* [17] optimized the internal structure of an aircraft wing by MDO method, Raymer *et al.* [18] presented the application of MDO to improve the aircraft conceptual design progress, Leifur *et al.* [19] applied the MDO method to the design of blended wing body transport aircraft with distributed propulsion, Juan *et al.* [20] discussed the multidisciplinary sonic-boom and minimization approach for supersonic aircraft, and Antoine *et al.* [21] proposed a MDO framework to optimize commercial aircraft with environmental performance. For small scale cost-effective Unmanned Aerial Vehicles (UAVs) design, such a sophisticated MDO design approach is usually not practical. To address this problem, Ganguli *et al.* [22] proposed a MDO approach to optimize the UAV wing aerodynamic configurations and its structure. Batill *et al.* [23] further considered the design of propulsion system in the MDO framework for UAVs design. In this work, the propeller is designed from scratch and then needs to be prototyped with extra cost and time consumption. Such a from-scratch propeller design method is not really necessary as a variety of off-the-shelf propellers of diverse size and specs are available thanks to the rapid porpulation of consumer drones during the last decade. To sum, all the past work on using MDO methods for aircrafts design are either designed for large aircrafts, or optimizing only single part (e.g. wing, propeller) for small-scale UAVs. A more systematic design methods that simultaneously design all involved UAV parts with consideration of practical constraints such as weight, geometry, propulsion system availability, etc. are not yet available.

In this paper, we propose a new optimization framework to design electric UAVs. When compared to [22, 23], our proposed framework optimizes both aerodynamic configurations (e.g. wingspan, aspect ratio, taper ratio, sweep angle) and propulsion systems (e.g. motor, propeller, battery). As such, this method gives a systematic way to simultaneously design all the key components in a UAV: from the wing, fuselage, to propulsion systems. Moreover, it naturally accounts for practical constraints arising from real world requirements, such as weight constraints and preliminary layout constraints from industrial design. The optimization framework is built on top of high-fidelity models on the UAV aerodynamics, motors, propellers

and batteries. These models are computationally cheap and highly accurate, as verified by intensive experiment data. To solve the optimization problem, which is NP hard due to its mixed-integer nature with both continuous and discrete optimization variables, a novel coordinate descent method is proposed and nicely decouples the continuous and discrete variables optimization. The coordinate descent method, as proved by trial designs, solves the optimization problem efficiently and reliably. Finally, a novel quadrotor tail-sitter VTOL UAV is designed, manufactured and tested to verify the efficacy of the proposed optimization framework. To sum, our contributions in this paper are fourfold: (1) an optimization framework for electric winged design; (2) high-fidelity experimentally-proved models of UAV aerodynamics, motors and propellers to accurately predict the performance of each component; (3) a coordinate descent method to solve the optimization problem effectively; (4) an efficient, portable quadrotor tail-sitter VTOL UAV designed by the proposed optimization framework.

This paper is an extended paper from a conference paper "A Coordinate Descent Method for Multidisciplinary Design Optimization of Electric-Powered Winged UAV", accepted in ICUAS 2018 [24]. In this paper, major new contributions are made: (1) we build a motor database based on the in-house experimental data, which is more accurate than the previous models based on the data retrieved from the manufacturer's website. (2) we perform analysis and trial designs to verify the robustness of the proposed coordinate descent method with respect to initial conditions; (3) we design transition and level flight controllers and test the designed tail-sitter VTOL UAV in level flight. The actual flight test performance fits to the predicted performance very well in both hover and level flights. This is the major and most notable contribution compared to our previous conference paper [24], where only hover flight test was conducted and hence only the hover performance was verified. With the level flight test, the entire framework is fully validated.

The rest of this paper is outlined as below. We will introduce the aerodynamic model and the propulsion system model in the Sect. 2 and Sect. 3, respectively. Based on these models, we formulate this UAV design problem as a general optimization problem in Sect. 4. After that, the mentioned coordinate descent method is proposed in Sect. 5 to solve this optimization problem. Then we use this optimization based design method to design a novel tail-sitter UAV. To validate the optimization result, we manufacture and test the designed UAV in Sect. 6. Finally, Sect. 7 concludes our work.

2 Aerodynamic Model

In this section, we present the aerodynamic model that will be used in the following optimization framework to calculate the aerodynamic force of a given UAV aerodynamic configuration. For an aircraft in level flight, its aerodynamic forces are mainly lift and drag forces, which are commonly parameterized by their respective coefficients as follows [25]:

$$L = \frac{1}{2}\rho V^2 S_{ref} C_L \tag{1a}$$

$$D = \frac{1}{2}\rho V^2 S_{ref} C_D, \tag{1b}$$

where C_L and C_D are the lift and drag coefficients respectively, V is the aircraft cruise speed, S_{ref} is the reference area, and ρ is the air density. In this section, we present the model of C_L and C_D of a given UAV aerodynamic configuration and validate these models with actual wind tunnel data of an existing model airplane. To compute the lift coefficient C_L, we suppose the aircraft is a monoplane with a single fuselage. As for the drag coefficient C_D, we divide it into three parts respectively caused by fuselage, wings, and protrusions, such as camera cover, landing gear, etc.

2.1 Lift

Wing is the main source of aerodynamic lift. At low angle of attack (AoA), the lift coefficient is usually linear to the angle of attack [26],

$$C_L = \alpha \cdot C_{L\alpha,WF} + C_{L0}, \tag{2}$$

where $C_{L\alpha,WF}$ represents the slope of aircraft lift curve considering wing-fuselage interference, C_{L0} denotes the lift coefficient at zero AoA. As suggested by [26], $C_{L\alpha,WF}$ can be expressed as:

$$C_{L\alpha,WF} = K_{WF} \cdot C_{L\alpha,W} \tag{3a}$$

$$K_{WF} = 1 + 0.025 \cdot \left(\frac{d_F}{b}\right) - 0.25 \cdot \left(\frac{d_F}{b}\right)^2 \tag{3b}$$

$$C_{L\alpha,W} = \frac{2\pi A}{2 + \sqrt{\frac{(2\pi A)^2}{C_{l\alpha,airfoil}{}^2}\left(\beta^2 + \tan \Lambda_{0.5}{}^2\right) + 4}}, \tag{3c}$$

where K_{WF} is the wing-fuselage interference factor. $C_{L\alpha,W}$ represents the slope of the airplane wing lift curve. d_F denotes the diameter of the fuselage cross-section, which is usually circular. A and b are the aspect ratio and the wing span respectively. $C_{l\alpha,airfoil}$ represents the slope of the two-dimensional wing airfoil lift curve. β is calculated from the March number $\beta = \sqrt{1 - M_a{}^2}$, and $\Lambda_{0.5}$ is known as the sweep angle of the 50% chord line. Readers can refer to classic aircraft design textbooks, such as [27] and [26] for a more comprehensive explanation on the terms mentioned above.

Although most of the terms in (3) are generated based on the aircraft configuration parameters (i.e., aircraft geometry parameters), the slope of two-dimensional airfoil lift curve determined by the given airfoil shape also plays an important role. For this purpose, we have established an airfoil database composed of 1115 common airfoils, such as GOE301, NACA2415, NACA0012, and MH60. For each airfoil, we calculate its two-dimensional lift coefficient (i.e. C_l) at different AoA by XFOIL [28] and fit a linear curve to obtain its slope $C_{l\alpha,airfoil}$.

2.2 Drag

After building the aerodynamic lift model, we continue to study the drag model, which is usually divided into the following three components [29]:

$$C_D = C_{D0} + C_{Di} + C_{D,others}, \tag{4}$$

where C_{D0} is the parasitic drag, C_{Di} represents the induced drag, these two components capture the drag of wing and fuselage. And $C_{D,others}$ denotes the drag caused by protruding objects (e.g., camera cover, landing gear, etc.)

Normally, the parasitic drag C_{D0} further breaks into three parts: form drag, friction drag, and interference drag [29], the model of these components have been intensively investigated in previous work [30, 29, 31]. In this paper, we adopt the parasitic drag model from Zhang,*et al.*[26], in which the parasitic drag consists of two parts: parasitic drag caused by wing (C_{D0W}) and fuselage (C_{D0F}), which are calculated via the formulas:

$$C_{D0,W} = C_f C_{FF,W} K_{FW} \frac{S_{wet,W}}{S_{ref}} \tag{5a}$$

$$C_{D0,F} = C_f C_{FF,F} K_{FW} \frac{S_{wet,F}}{S_{ref}}, \tag{5b}$$

where $C_f = 0.074 \cdot \sqrt[-0.2]{R_e}$ is the friction coefficient [32], R_e is the Reynolds number. S_{ref} denotes the UAV reference area. $C_{FF,W}$ and $C_{FF,F}$ present the form factors for wing ($C_{FF,W} = 1 + L\left(\frac{t}{c}\right) + 100\left(\frac{t}{c}\right)^4$ [33]) and fuselage ($C_{FF,F} = 1 + \frac{2.2}{(l/d)^{1.5}} + \frac{3.8}{(l/d)^3}$ [34]), respectively. $S_{wet,W}$ and $S_{wet,F}$ represent the respective wetted area of the wing and fuselage.

Another component of the total drag in (4) is induced drag C_{Di}, which is a particularly crucial part because it accounts nearly half of the total drag in most cases. Similar to parasitic drag, there are many studies to simulate the induced drag, such as Trefftz planes theory [35], vortex lattice methods [36], and Prandtl's lifting-line theory [37]. In this paper, we formulate the induced drag according to the method proposed in [38], which applies to subsonic aircraft with straight-tapered, twisted, swept back wings, which is our case.

$$C_{Di} = \frac{{C_L}^2}{\pi A e} + C_L \theta C_{L\alpha,airfoil} \nu + (\theta C_{L\alpha,airfoil})^2 \omega, \tag{6}$$

where e and θ represent the Oswald efficiency and the wing twist angle respectively, $C_{L\alpha,airfoil}$ is the slope of the two-dimensional airfoil lift curve as mentioned in (3c). For twisted wing (non-zeros θ), ν and ω are respectively the linear and quadratic terms of induced drag caused by twisting.

In addition to the induced drag and parasitic drag on wing and fuselage, another source of drag is protuberance drag, which is generated by protruding objects. To simplify the protuberance drag model, we consider these protruding objects as standard geometrics, such as cylinder, ball and aircraft capony [26]:

$$C_{D,cylinder} = 0.628\left(\frac{l}{d}\right)^{0.1202} \cos\left(1.2255\left(90^\circ - \theta\right)\right) \tag{7a}$$

$$C_{D,capony} = \Delta\frac{S_c}{S_{ref}}, \tag{7b}$$

where $C_{D,cylinder}$ is the drag generated by the cylinder, its length and diameter are expressed as l and d, respectively. θ is the angle of inclination between the air flow and the axis of the cylinder. And $C_{D,capony}$ is the drag coefficient of the aircraft capony, calculated by the capony drag coefficient increment Δ, the maximum cross-section area of the aircraft capony S_c and the reference area S_{ref}.

2.3 Validation on an Existing Airframe

To verify the proposed aerodynamic model in previous sections, we conduct a full scale wind tunnel test on an existing aircraft and compare the results with that predicted by our proposed model. The existing aircraft is a vertical take-off (VTOL) tail sitter UAV [39], which is reconstructed from a commercial off-the-shelf model airplane known as Skywalker X5. Fig. 1 shows the geometric configuration of the aircraft, which consists of three main parts: wings, fuselage and landing gears. The landing gears also serve as motor mounts and are symmetrically assembled around the fuselage. The details of the aircraft design is described in [39]. The leading gears are modeled as cylinders when calculating their drags.

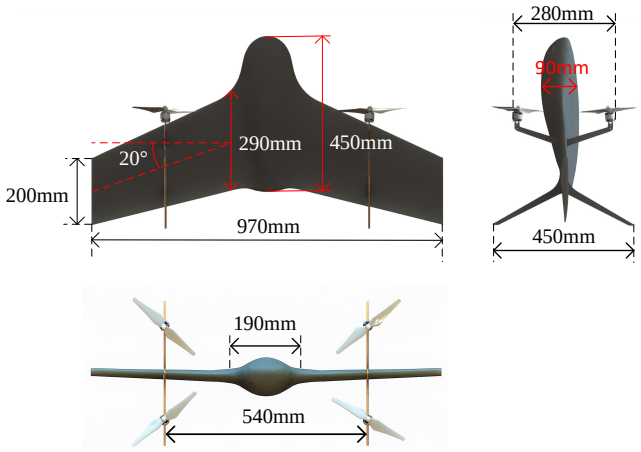

Fig. 1 The physical dimension of "Tail Sitter UAV X5"

Fig. 2 shows the wind tunnel test configurations, which is detailed in our previous work [40]. Fig. 3, Fig. 4 and Fig. 5 respectively show lift coefficient, drag coefficient and lift-drag polar, measured by wind tunnel test (marked with a red cross) and calculated by aerodynamic model (marked as blue diamond). In the wind tunnel test, for each AoA, different wind speeds are tested. As the airspeed

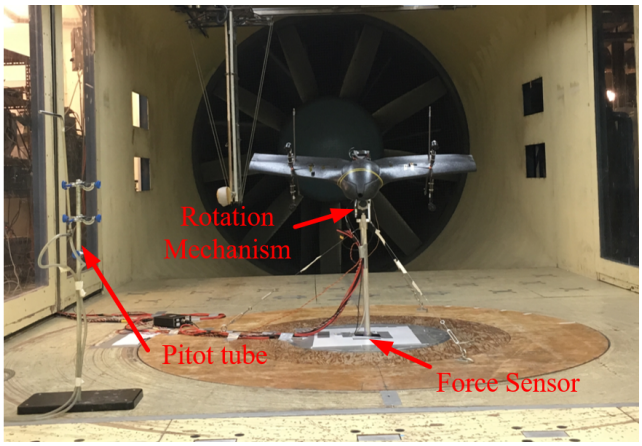

Fig. 2 Wind tunnel test

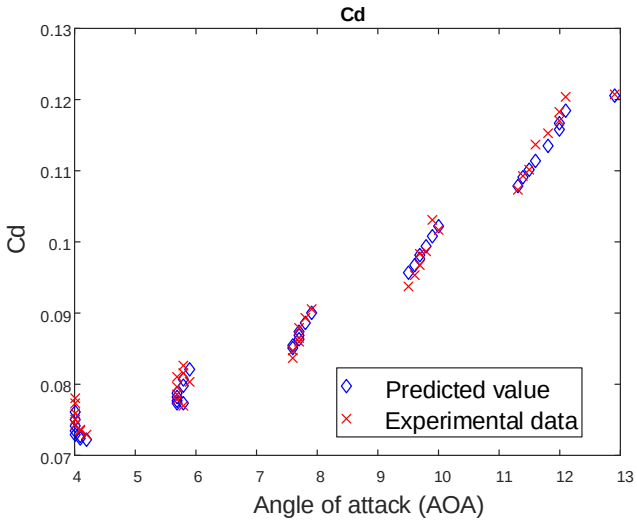

Fig. 3 Drag coefficient

increases, the attitude of the aircraft is slightly disturbed due to the non-rigidity and deformation of the aircraft. As a result, the AoA slightly drifts away from its set point, which is observed as distinguishable AoA clusters in these figures. It should also be noted that the measured lift coefficient varies with different airspeeds even at similar AoA, especially at 6° AoA. This variation may be due to boundary layer separation with low Reynolds number or measurement errors. From Fig. 3 – Fig. 5, it can be seen that the predicted drag coefficient almost perfectly fits the experimental data, and the predicted lift drag ratio and lift coefficient are slightly lower than the experimental data. These prediction accuracy is quite satisfactory for our design purpose as shown in the following sections.

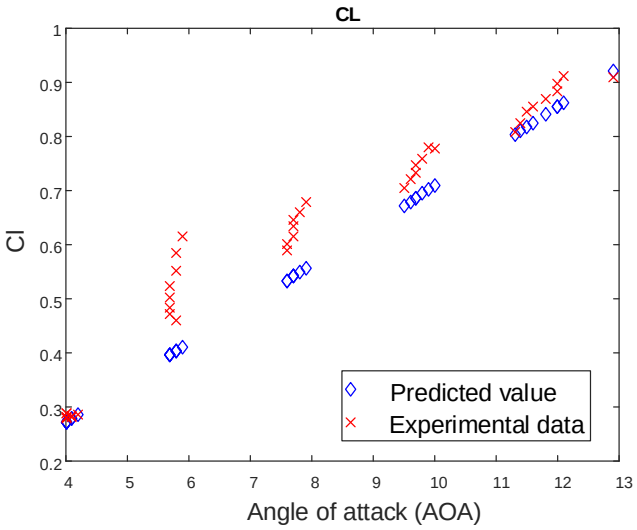

Fig. 4 Lift coefficient

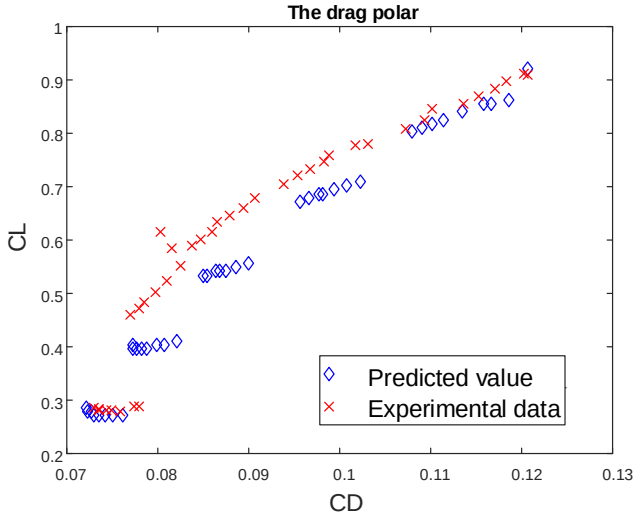

Fig. 5 Lift to drag ratio

3 Propulsion System Model

For small electric UAVs, the propulsion system is composed of three parts: propeller, motor, and battery. This chapter will introduce how to predict the flight range or endurance by combining these three components together. To do so, accurate models of propeller, motor and battery are necessary. The details are shown as follows.

3.1 Propeller Model

In this paper, we consider the UAV design based on off-the-shelf propulsion system (i.e. propeller, motor and battery) instead of designing any of these components from scratch. Thanks to the large population of quadrotor UAVs in recent decades, a wide range of propellers and motors with different specs are available to use. The manufacturers even tested their performance and made them public accessible to ease designers. In this section, we make use of these data and build a database of propellers and motors. We also present models to interpolate these database such that their performance can be evaluated with any external load and any combinations of propeller, motor and battery.

The propeller thrust T and torque Q are usually parameterized by their dimensionless coefficients C_T and C_Q respectively [41]:

$$J = \frac{V}{nD} \tag{8a}$$

$$C_T = \frac{T}{\rho n^2 d^4} \tag{8b}$$

$$C_Q = \frac{Q}{\rho n^2 d^5}, \tag{8c}$$

where V is the axial speed of the propeller (air flow along the propeller rotation axis), which is also the cruising airspeed for the UAV in level flight. d is the propeller diameter. n denotes the rotational speed in Hertz (that is, the rotation per second). ρ denotes the air density. J represents the dimensionless parameter advanced ratio. C_T and C_Q are propeller thrust and torque coefficients which are dimensionless parameters of thrust T and torque Q, respectively. Using these parameterization J, C_T, and C_Q, a group of propeller performance data evaluated by APC is shown in Table 1.

Table 1 Sunnysky A2212 (980KV) test data

Propeller RPM = 5000							
V (mph)	J (Adv Ratio)	Pe	Ct	Cp	PWR (Hp)	Torque (In-Lbf)	Thrust (Lbf)
0.0	0.00	0.0000	0.1769	0.1084	0.003	0.043	0.088
1.0	0.04	0.0649	0.1763	0.1103	0.003	0.044	0.088
1.9	0.08	0.1270	0.1755	0.1121	0.004	0.044	0.087
2.9	0.12	0.1865	0.1746	0.1140	0.004	0.045	0.087
3.8	0.16	0.2431	0.1736	0.1159	0.004	0.046	0.086

With the provided propeller performance data, we fit a smoothed spline model to the non-dimensional coefficients C_T and C_Q with respect to the J at every rotational speed in revolution per minute(RPM). Fig. 6 and Fig. 7 respectively shows the fitted C_T and C_Q of the propeller APC 9×6E. It is seen that the fitting accuracy is quite satisfactory. To evaluate the C_T and C_Q at an arbitrary RPM, first order interpolation is used. As a result, a model of $C_T(J, RPM)$ and $C_Q(J, RPM)$ is obtained for each propeller and enables us to evaluate the propeller

thrust and torque for any given propeller RPM and axial speed. We apply the above fitting method to 414 APC propellers with their provided propeller performance data [42]. These 414 propellers are of different specs and constitute a diverse database for the following optimization to choose from. This database can be enriched further when more propeller test data are available.

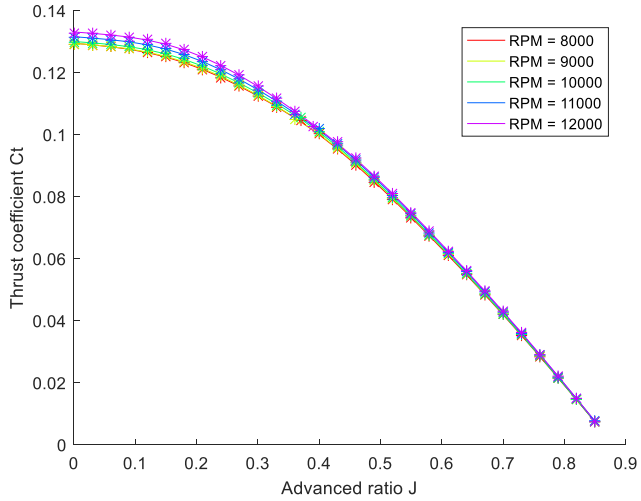

Fig. 6 The raw data versus fitted curve of C_T and J

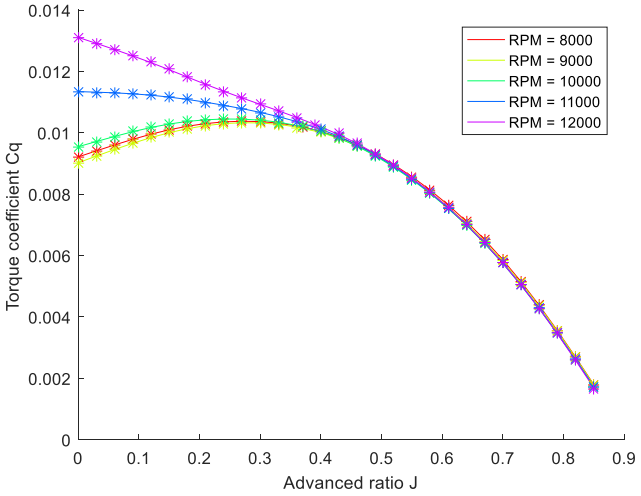

Fig. 7 The raw data versus fitted curve of C_Q and J

Finally, the propeller consumes power by providing thrust, which is necessary to compensate the aerodynamic drag. To compute the propeller power consumption,

we first compute the required RPM such that a thrust T (T is equal to the drag D) is generated at level speed V. This poses a nonlinear equation in the form of $C_T((60 \cdot V)/(x \cdot d)), x) \cdot \rho n^2 d^4 = D$, where x is the propeller rotation speed in RPM to be solved and C_T is a known function fitted above with two inputs: advanced ratio $60 \cdot V/(x \cdot d)$ and the propeller rotation speed x. Noticing that the propeller thrust T is monotonically increasing with x, we implement a bisection search to solve this nonlinear equation. With the solved rotation speed, the propeller torque Q is easily computed by invoking the known propeller model C_Q fitted above. To sum, in evaluating the propeller power, the propeller module takes drag and level speed as inputs and outputs the propeller torque and rotation speed. The torque and rotation speed will further be fed to motor module to compute the motor power consumption. Fig. 8 shows one of the propeller module output, propeller torque, as a function of its inputs, thrust/drag and level speed.

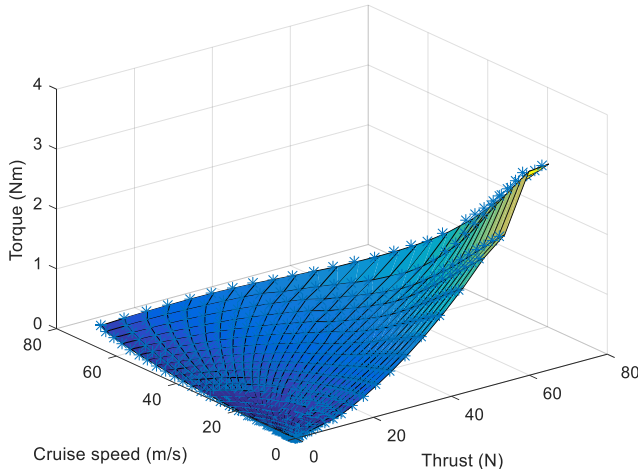

Fig. 8 The raw data and fitted surface of torque, velocity and thrust

3.2 Motor Model

For brushless DC (BLDC) motors considered in this paper, their current and voltage at steady state are related to the rotation speed and torque load by the following equations.

$$I = K_i \tau \tag{9a}$$

$$U = K_v \omega, \tag{9b}$$

where τ is the torque produced by motor, also named motor load. And ω denotes the rotational speed in rad/s ($\omega = \text{RPM} \cdot \frac{2\pi}{60}$). K_i and K_v are motor torque constants and speed constants, respectively. U and I denote voltage and current, respectively.

Based on the baseline model in (9), we further propose a more practical model by considering more minor effects, which prove to fit actual test data more accurately than the baseline model. The model is proposed as follows.

$$I = K_i \left(Q + b \cdot \omega + b_0\right) \tag{10a}$$

$$U = K_v \omega + I \left(r_0 + r \cdot \omega\right) \tag{10b}$$

$$P_{required} = U \cdot I, \tag{10c}$$

where Q is the propeller torque computed from the propeller module. b is the column friction torque coefficient and b_0 is a static friction torque of the motor. r_0 is the armature resistance and $r \cdot \omega$ denotes the resistance increment due to armature heating, which is assumed to be proportional to rotation speed by constant r.

To fit the motor model in (10), we test the performance of several common motors combined with propellers. Fig. 9 shows the motor test apparatus we have developed to measure the motor parameters, where we use a 6-dimensional force sensor to capture the torque and thrust generated by the propeller simultaneously. During the experiment, we also record the current and voltage drained from the power supplier. As can be seen, this test apparatus is lack of intake air, we can therefore only measure the static force of the propeller, but this is sufficient to estimate the motor parameters in (10). The reason we test the motor together with a propeller is that most motor manufacturers provide motor test data with a specific propeller, so our test data will be compatible with those data provided by motor manufacturer. One can also test a motor independently and fit its parameters in (10) wherever possible.

Table 2 Sunnysky A2212 (980KV) test data

Prop(inch)	Volts(V)	Amps(A)	Thrust(gf)	Watts(W)	Efficiency(g/W)
APC9×6E	15.2	0.2	44.90	3.04	14.77
		0.8	131.08	12.16	10.78
		2.0	242.28	30.40	7.97
		3.7	370.59	56.24	6.59
		6.0	512.99	91.20	5.62
		8.9	672.30	135.28	4.97
		12.1	774.27	183.92	4.21

In this paper, we test six motors in total. As an example, Table 2 shows the measured data for the motor "$SunnyskyA2212(980KV)$" with the propeller "$APC9 \times 6E$". To estimate the motor parameter, we first compute the propeller torque and rotation speed from its thrust and axial speed, which is zero, from the propeller module as described in the propeller subsection. With the calculated propeller torque and rotation speed, and also the recorded voltage and current, we fit the motor parameters in (10) by least square fitting. With the motor parameter, its voltage, current and power consumptions can be evaluated from the inputs: load torque (i.e. the propeller torque) and rotation speed. Fig. 10 shows the power consumption predicted by motor module versus of measurements. It can be seen that the model predictions fit to the experimental data very well. We should also remark that although we test only 6 motors coupled with propellers,

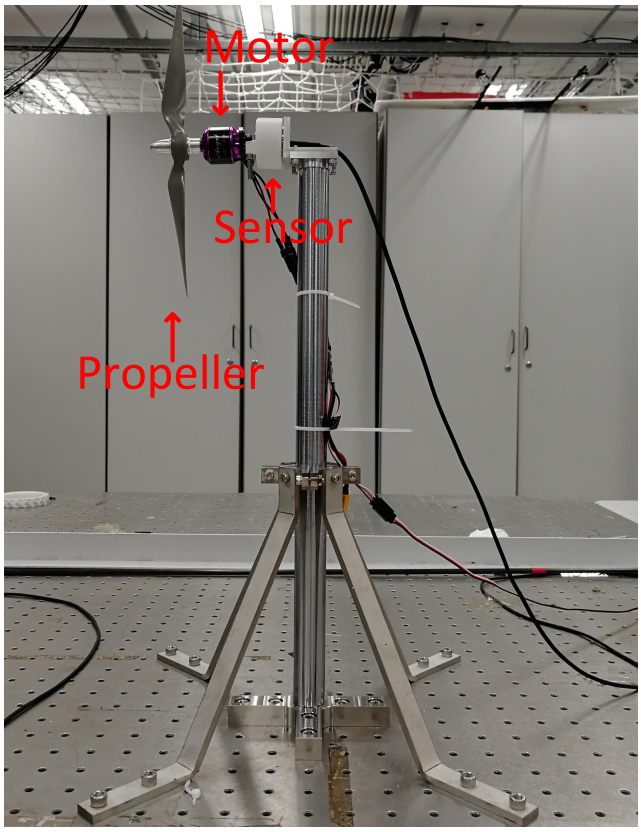

Fig. 9 The experiment apparatus for motor testing

other test method or more motor data if available can be naturally incorporated into the motor database. The extended motor database provides more choices for the UAV optimization in the following sections.

3.3 Battery Model

The last piece of component is the battery, whose discharge time is immediately the flight endurance and also implies the flight range when multiplied with the level flight speed. In this paper, we use a Li-Po battery model proposed by Traub *et al.* [43], which proves to be rather accurate in our case. In the Li-Po battery model, the discharge time is estimated by the following formula.

$$t = \frac{R_t}{I^n}\left(\frac{C}{R_t}\right)^n, \tag{11}$$

where C denotes the battery capacity in ampere-hour Ah. The R_t is a constant parameter named battery hour rating in hour h, whose value is usually 1 for portable batteries [43]. And n represents a discharge parameter, which depends on battery type and the temperature. According to the results of L.W. Traub's

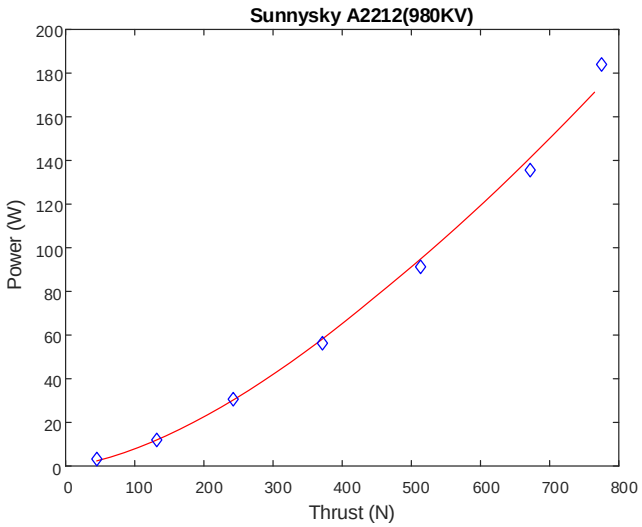

Fig. 10 Motor power predicted by model and that of experiments

experiment in [43], its value is usually 1.22. I denotes the battery discharge current calculated as

$$I = P_{required}/U, \tag{12}$$

where $P_{required}$ is the power drained from the battery. In our study, $P_{required}$ is the motor power consumption and calculated from the motor module. U is the instantaneous voltage applied to the battery to generate the instantaneous current I through the battery. Accurately tracking the instantaneous current and voltage of a battery is usually prohibitive, L.W. Traub [43] demonstrated that the average voltage and current can be used as replacements to produce relatively accurate discharge time in (11).

4 Formulation of UAV Design Optimization

Based on the model of UAV aerodynamics configuration and propulsion system outlined previously, which enable us to evaluate an UAV performance (in terms of flight range, endurance, or any other specs) for a given aerodynamic configuration and specific propulsion system combination, we cast the UAV design problem as an optimization problem, as follows.

$$\begin{array}{ll} \min_{x\in\mathbb{R}^n, z\in\mathbb{S}} & l_0(x,z) \\ \text{s.t.} & L(x) = W \\ & l_i(x) \leq 0, \end{array} \tag{13}$$

where optimization vector x (in dimension of n) is the stack of all aerodynamic configuration variables (e.g., wingspan b, taper ratio A, sweep angle λ, the angle of attack α, wing chord at root c_{root}, cruising airspeed V, etc.). These variables are real numbers, or continuous variables by their natures. The other optimization

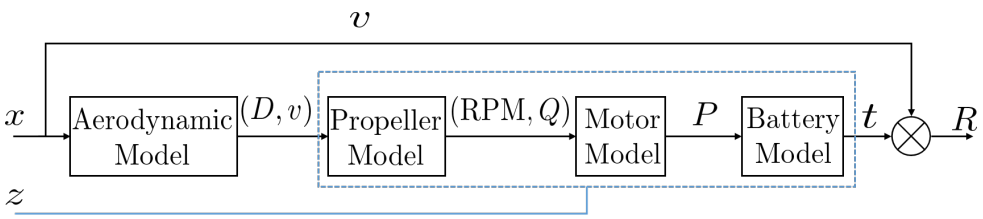

Fig. 11 Evaluation of the aircraft flight endurance or range

variable z denotes the propulsion system. Since the types of off-the-shelf motors and propellers are countable, variable z is really an index (a discrete variable) denoting a specific propulsion system combination, which consists of motor index and propeller index. Therefore, S, the domain of z, is a countable set representing the collection of all available combinations of propulsion system with the quantity K. For example, in our current implementation, the number of all available motors and propellers are 6 and 414, respectively, then $K = 414 \times 6 = 2484$. $l_0(x, z)$ is the objective function that designers want to optimize. It can be flight endurance, flight range, or any specs depending on the designers' requirement. The first constraint of (13), $L(x) = W$, means that the lift $L(x)$ should be equal to the UAV gravity to maintain a stable level flight, where $L(x)$ is determined by the UAV aerodynamic configurations x from the previous aerodynamic models. The remaining constraints of (13), $l_i(x)$ may be derived from other practical constraints, such as size constraints and preliminary layout constraints from the industrial design. It should be remarked that these constraints depend only on the aerodynamic configurations x in most cases. We will make use of this fact in the following sections to ease the optimization solver.

To define the objective function $l_0(x, z)$ in (13), we take an example where the flight range is to be optimized. Fig. 11 shows the procedures to calculate the flight range $l_0(x, z)$ for a given UAV aerodynamic configuration x and propulsion system z: first, the drag D should be determined from x (which contains the level speed v) from the previous aerodynamic models. The drag D and level speed v are then fed to the propulsion system z (the dashed blued box in Fig. 11) to determine the battery discharge time. To do so, the propulsion system first calculates the propeller torque and rotation speed from the inputed drag (i.e. propeller thrust) and level speed (i.e. propeller axial speed) by invoking the propeller model. Then the propeller torque and speed are fed to the motor model to calculate the motor power consumption, which is finally used by the battery model to determine its discharge time. Then with the level speed v and discharge time t, the flight range is easily determined. If the flight endurance is being optimized, the discharge time t would be used instead as the output of $l_0(x, z)$.

5 Coordinate Descent Optimization

As can be seen, the original function in (13) involves both discrete variables z and continuous variables x, which results in a mixed-integer optimization problem that is NP hard [44]. To deal with this problem, we rewrite the optimization problem in (13) into the following equivalent form:

$$\begin{array}{ll} \min_{x\in\mathbb{R}^n} & l_0(x,z) \\ \text{s.t.} & L(x)=W \\ & l_i(x)\le 0 \\ & z\in\mathbb{S} \end{array} \tag{14}$$

where the domain of variable z, $z \in S$, is rewritten as an explicit constraint of the optimization problem. With this form, it is clearly seen that the constraints for continues variable x, the aerodynamic configuration, and discrete variable z, the propulsion system, are really decoupled. This decoupling feature enables us to optimize $l_0(x, z)$ with respect to only one variable (x or z) at a time, as shown in Fig. 12.

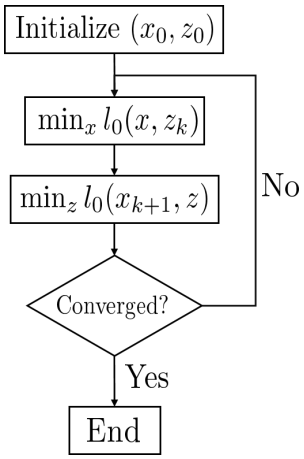

Fig. 12 Coordinate descent method for UAV design optimization

Procedure 1: Optimize the continuous variable x (i.e., aircraft configuration parameters) while fixing the other variable z, the propulsion system, at its latest optimal value z_k. That is,

$$\begin{array}{ll} \min_{x\in\mathbb{R}^n} & l_0(x,z_k) \\ \text{s.t.} & L(x)=W \\ & l_i(x)\le 0 \end{array} \tag{15}$$

The function (15) is a nonlinear optimization problem involving only the continuous variable x, so it can be optimized by a general nonlinear optimization solver, such as the sequential quadratic programming method [45] or interior point method [46].

Procedure 2: Optimize the discrete variable z (i.e., the combination of propulsion system)while fixing the other variable x, the aerodynamic configuration, at its latest optimal value x_{k+1}. That is,

$$\begin{array}{ll} \min_{z} & l_0(x_{k+1},z) \\ \text{s.t.} & T=D(x_{k+1}) \\ & z\in\mathbb{S} \end{array} \tag{16}$$

where T denotes the thrust generated by the propeller candidate. $D(x)$ represents the aerodynamic drag calculated from the aerodynamic model for the given aerodynamic configuration x_{k+1}. Since the quantities of all possible propulsion system combinations are limited and countable, we use brute force search and calculate the objective function for every propulsion system combination, among which the best one is selected.

We iterate the two procedures until convergence (i.e., the optimal aerodynamic configuration x and propulsion system z at the current iteration are identical to that of the last iteration). This alternative optimization process is called block coordinate descent optimization (there are two blocks: one is x in $\mathbb{R}^n$, and the other one is z in $\mathbb{S}$) [47]. Although the non-convex subproblem in procedure 1 and the mixed integer optimization nature [48] lead to no guaranteed convergence property in theory, the proposed method works very efficiently and reliably in practice. As shown in Sect. 6, it only takes 2 or 3 iterations to converge for most cases. In addition, it always converges to the same optimal solution regardless of the initial conditions.

6 Case Study

Our proposed optimization based UAV design framework and the coordinate descent method provide a powerful tool for the evaluation and optimization of electric UAVs with single-wing. As introduced in the Sect. 2 and Sect. 3, the aerodynamic model and propulsion system model have been verified independently. In this section, we use this framework to design an optimal quadrotor tail-sitter VTOL UAV (Sect. 6.1). The designed UAV specs are verified by both CFD simulations (Sect. 6.2) and actual flight data acquired from the UAV prototype, which is manufactured according to the optimal design (Sect. 6.3).

6.1 Aircraft Conceptual Design

To verify the effectiveness of the proposed UAV design optimization framework, we use it to design an efficient, highly maneuverable and portable UAV. It is commonly understood that, multi-rotor UAVs have high mobility and maneuverability, but they suffer from low flight efficiency, thus short range or endurance. On the other hand, fixed-wing airplanes can achieve higher efficiency, but require runway or catapult to take off or land. To achieve both the maneuverability and efficiency, we aim to design a vertical take-off and landing (VTOL) airplane. More specifically, we design a quadrotor tail-sitter VTOL UAV due to its superior mechanical simplicity and flight flexibility compared to other types of VTOL UAVs [49].

Table 3 Model parameters

Battery discharge parameter n	1.22	Wing twist θ	0°
Battery hour rating R_t	1	Air density ρ	$1.184 kg/m^3$
Battery capacity C	$4.5Ah$	Battery manufacturer	DJI

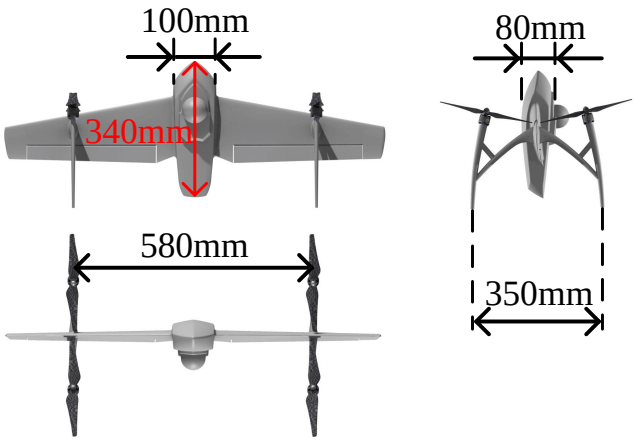

Fig. 13 Constant parameters of tail-sitter UAV under design

The UAV is assumed to be 2kg according to our prior UAV development experiences. And a 4 cell battery with capacity of 4.5 Ah is used. Other parameters used in the optimization framework are summarized in Table 3. Besides these configurations, Fig. 13 shows the basic layout of the UAV to be designed. In our design, we fix the landing gear location and the size of fuselage at constant values. The variables to be optimized consist of 6 UAV aerodynamic configuration parameters (denoted as $x \in \mathbb{R}^6$) and a countable propulsion system index (denoted as z). The 6 aerodynamic parameters are wingspan, taper ratio, sweep angle, AoA, wing chord at root and cruising airspeed. Some of these are illustrated in Fig. 14. With practical constraints on portability and industrial design, these 6 parameters are within ranges specified in the Table 4. The propulsion system index is one of the 2484 propulsion system combinations (i.e. 6 motors multiplied by 414 propellers as mentioned previously). In addition, taking into account the size of the aircraft, the propeller diameter is limited to 9 inches.

Table 4 Constraints of the configuration parameters

	Upper bound	Lower bound
Wing span (m)	0.9	0.5
Taper ratio	0.48	0.3
sweep angle (°)	9	6
Angle of attack (°)	7	0
Root chord of wing (m)	0.2	0.06
Velocity (m/s)	25	3
Propeller radius (inch)	9	N.A.

The optimization objective concerned in this example is the mixed flight endurance where for 10% of time the UAV is hovering to account for the vertical takeoff and landing phase and for the rest 90% of time the UAV is at level flight to account for the efficient mission phase. The initial values of the optimization variables are randomly distributed within their respective ranges.

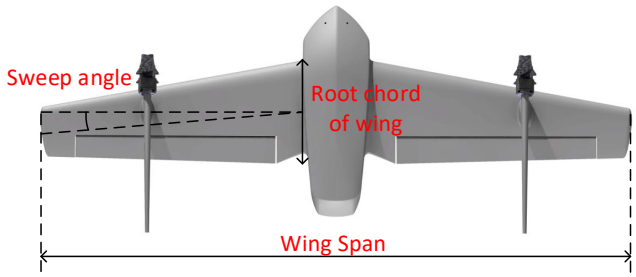

Fig. 14 Partial tunable parameters of the tail-sitter UAV

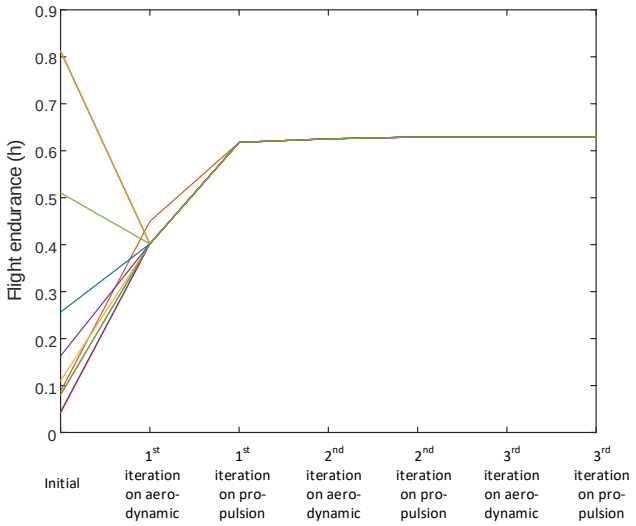

Fig. 15 Objective function iterate with different initial value

With the coordinate descent method proposed previously, the UAV aerodynamic configuration (x) and propulsion system (z) are alternatively optimized. The optimization processes for 10 different random initial conditions are shown in Fig. 15. The x axis denotes the optimization iterations over either aerodynamic configuration x or propulsions system z. y axis represents the values of objective function (i.e., mixed flight endurance here) at that iteration. It is seen in Fig. 15 that the mixed flight endurance (i.e., the negative objective function) after the first iteration of optimization may decrease from its initial condition. This is because the initial conditions are randomly generated within their respective ranges, so they may not a feasible solution at all (i.e., $L(x) = W$ is not satisfied). Excluding the unfeasible initial conditions, the objective function is monotonically decreasing for the rest iterations. It is also seen that for all initial conditions, the objective function converge to the same optimal value with the same optimal solution although the optimization (sub-)problem is not convex. This proves the reliability of the proposed coordinate descent method.

Table 5 summarizes the optimal aerodynamic configurations and propulsion system returned by the coordinate descent solver. It can be seen that, with the

Table 5 Optimal aircraft configuration

Propeller name	APC9x6E
Motor name	Sunnysky A2212 (980KV)
Wing span	0.90 m
Taper ratio	0.48
sweep angle	7.30°
Angle of attack	7.00°
Root chord of wing	0.20 m
Cruise speed	12.53 m/s
Current at hover status	22.95 A
Current at level fly status	4.76 A
Power at hover status	364.96 W
Power at level fly status	75.67 W
Flight endurance at hover status	8.22 min
Flight endurance at level fly status	56.03 min
Mixed flight endurance	37.75 min
Mixed flight range	28.39 Km
Lift to drag ratio	6.7421

optimal UAV configuration, the mixed flight range is up to 28.39 km and the mixed flight endurance is 37.75 min. At the same time, we find a significant power increment from level flight mode to hover mode, which is the intrinsic property of the tail-sitter UAV. We also notice that some optimization variables (e.g., taper ratio, wingspan, wing root chords and AoA) reach their respective upper bounds. This is because that increasing these parameters will lead to the growth of lift-drag ratios, as suggested in the Sect. 2.

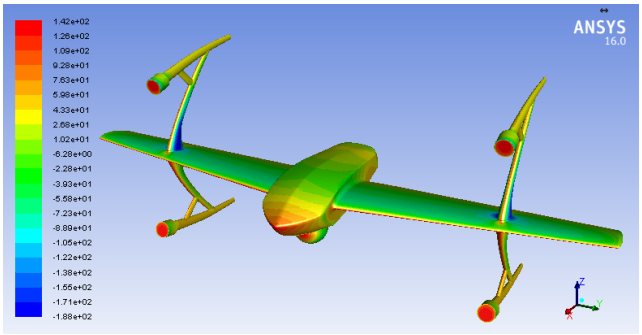

Fig. 16 The pressure distribution contour of the designed tail sitter

6.2 Comparison with CFD Analysis

To validate the UAV designed previously, we perform a 3D CFD analysis by ANSYS and compare the results with the optimization results in Table 5. In the CFD analysis, 3,920,188 tetrahedral meshes and 2,047,179 pentahedral meshes are used. All configuration settings with low speed, incompressible flowing air are applied,

with airspeed set at 12.53 m/s, which is the cruising airspeed returned by the optimization above. The solver for CFD analysis is pressure-velocity coupled SIMPLEC solver.

The CFD analysis shows that the lift drag ratio is 6.6357, which is almost identical to the lift drag ratio generated by our optimization framework (Table 5); the error is only 1.58%. Fig. 16 shows the pressure distribution contour produced by ANSYS, where the pressure is between 142 Pa and -188 Pa.

6.3 UAV Manufacturing and Actual Flight Tests

6.3.1 Manufacturing and Functionality Test

In order to manufacture the UAV designed in Sect. 6.1, we machined a set of molds by a CNC machine and then use these molds to manufacture the aircraft by carbon fiber. The manufactured components are finally assembled with propulsion system, avionics system, battery and servos. A 4s Li-Po battery "Phantom 3 Intelligent Flight Battery", manufactured by DJI, is adopted for our UAV prototype, since its capacity(4480mAh) is closed to our design constraint(4500mAh). As for the servo, we selected "ES08DE (8g) Digital Servo", which is manufactured by EMAX and the specifications are detailed in Table 6. The final UAV in operation is shown in Fig. 17 and Fig. 19, the total weight of the final UAV, including all onboard electronic equipment, sensors, propellers, motors, and electronic speed controllers (ESC), etc., is 1.6 kg, leaving a room of 400g for payload. The UAV has been intensively tested in actual outdoor flight experiments to verify its functionality, including take-off, hover, forward and backward transition and land.

Table 6 Specifications of the chosen servo

Size	Weight	Operation Voltage	Stall torque	Operation speed
$23 \times 11.5 \times 24$ mm	8.6 g	4.8 V -6 V	1.6 kgf.cm	0.12 sec/60°

6.3.2 Hover Test

To verify the UAV power consumption in hover mode, we perform a hover flight test where the UAV hovers at a stationary point right after take-off until all the battery power is exhausted. This test is implemented in a room of $5m(width) \times 8m(length) \times 3m(height)$ without disturbance, as shown in Fig. 17. During the test, we add an extra payload such that the total UAV weight is as designed (i.e. 2kg). Fig. 18 shows the battery current during the entire flight. It is seen that the average current is around $23.38A$ and the hover endurance is $8.38min$, which are very close to the predicted value shown in the Table 5. The error between predicted value and actual tested value of average current and hover endurance are 1.87% and 1.94% respectively. The small deviation may be caused by the small error between the fitted model and the actual performance. In addition, wing-propeller interaction, ground effect, and measuring error may also contribute to the deviation. In spite of these, these results show that the proposed propulsion

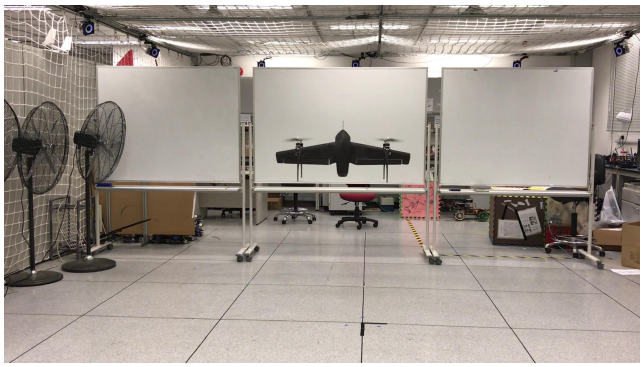

Fig. 17 Indoor flight environment

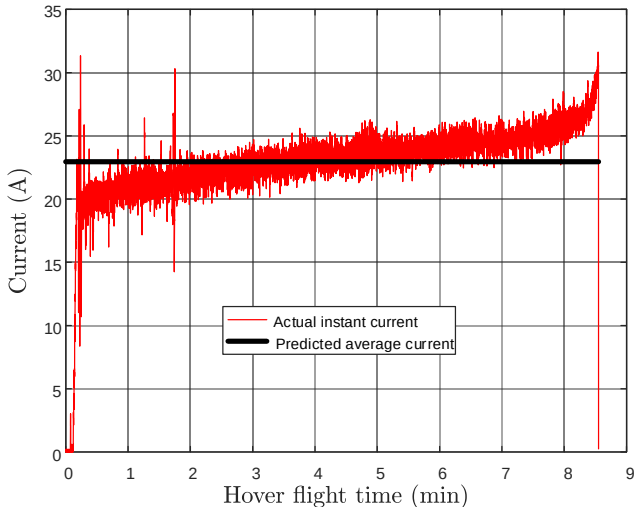

Fig. 18 Current of the indoor flight experiment

system model can predict the hover performance very accurately and therefore the designed UAV has the promised hover performance.

6.3.3 Level Flight Test

To verify the UAV performance in level flight, we perform an outdoor flight test in a wide open space of $500m \times 600m$ as shown in Fig. 19. It is a cloudy day with a breeze (under 3.3m/s) and the temperature is between $25°C \sim 28°C$. Similar to the hover test, the UAV has a total weight of 2kg by adding extra payloads.

Fig. 20 shows the flight log of the test. The lower figure shows the pitch angle which indicates the different flight modes during the test: from 290s to 300s, the UAV is at hover mode where the pitch angle is zero. From 302s to 308s, the UAV is in its transition to level flight. During this period, the pitch angle is monotonically decreasing and the flight speed is monotonically increasing accordingly. From 310s to 337s, the UAV is in steady level flight where both the angle of attack and

Fig. 19 Outdoor flight experiment

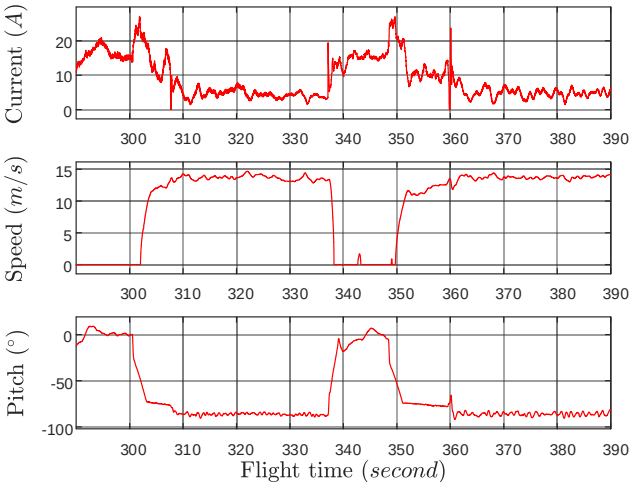

Fig. 20 Current, speed and pitch of the outdoor flight test

the flight speed are well maintained around their respective values. At 337s, the UAV transits back to hover and the speed decreases to zero. After that, another transition is performed and the procedure is quite consistent with the prior one. It can be seen that in steady level flight, the speed is 13.67m/s and the current fluctuates between 7.59A and 1.36A, with an average current equal to 4.42A. When compare to their designed values in Table 5, the current error is as small as 7.14%, which may be caused by cross wind and the aerodynamic modeling error. Such a small error proves the accuracy of our aerodynamic model and justifies the effectiveness of the proposed design optimization framework.

Also, based on the power consumption in hover mode (see Sect.6.3.2) and level flight mode (see Sect. 6.3.3), we can calculate the mixed flight endurance, where 10 % of time is for hover, and 90% of the time is for level flight. The calculated mixed flight endurance is $39.68min$, which is close to the predicted flight endurance of $37.75min$, with an error of 5.11%.

7 Conclusion

In this paper, we presented comprehensive models to model each component of a winged UAV: aerodynamic model for wing and fuselage, propeller model, motor model and battery model. Each of these models was verified by actual test data either collected by our own or from other sources. With the accurate models, we proposed an optimization based UAV design framework. In our framework, the UAV design problem is cast into an optimization problem where both the UAV aerodynamic configuration and propulsion system are designed by optimization. The proposed optimization framework also naturally took practical constraints such as weight, size, and industrial design. Furthermore, to solve the posed optimization problem, we proposed a coordinate descent method, which proved to be rather efficiently and reliably by trial design tests. Finally, using the proposed optimization framework, we designed a novel portable and highly efficient quadrotor tail-sitter VTOL UAV. The designed VTOL UAV was manufactured and tested. Test results verified the UAV design specs in both hover and level flight, thus validating the effectiveness of the proposed UAV design optimization framework.

References

1. Kuchemann, D.: The aerodynamic design of aircraft. Progress in aeronautical sciences, 1965, 6,271 (Pergamon, London) (1978)
2. Niu, C.: Airframe structural design: practical design information and data on aircraft structures. Conmilit Press (1988)
3. Oates, G.C.: Aircraft propulsion systems technology and design. Aiaa (1989)
4. Vatistas, G.H., Lin, S., Kwok, C.K.: Reverse flow radius in vortex chambers. AIAA Journal **24**(11), 1872, 1873 (1986). DOI 10.2514/3.13046
5. Goraj, Z., Cisowski, J., Frydrychewicz, A., Grendysa, W., Jonas, M.: Mini uav design and optimization for long endurance mission. In: Proceedings of ICAS Congress (2008)
6. Gu, H., Lyu, X., Li, Z., Shen, S., Zhang, F.: Development and experimental verification of a hybrid vertical take-off and landing (vtol) unmanned aerial vehicle (uav). In: Unmanned Aircraft Systems (ICUAS), 2017 International Conference on, pp. 160–169. IEEE (2017)
7. Martins, J.R., Lambe, A.B.: Multidisciplinary design optimization: a survey of architectures. AIAA journal **51**(9), 2049–2075 (2013)
8. Ebrahimi, M., Farmani, M.R., Roshanian, J.: Multidisciplinary design of a small satellite launch vehicle using particle swarm optimization. Structural and Multidisciplinary Optimization **44**(6), 773–784 (2011)
9. Hwang, J.T., Lee, D.Y., Cutler, J.W., Martins, J.R.: Large-scale multidisciplinary optimization of a small satellites design and operation. Journal of Spacecraft and Rockets **51**(5), 1648–1663 (2014)
10. Ashuri, T., Zaaijer, M.B., Martins, J.R., Van Bussel, G.J., Van Kuik, G.A.: Multidisciplinary design optimization of offshore wind turbines for minimum levelized cost of energy. Renewable Energy **68**, 893–905 (2014)
11. Zi, B., Ding, H., Cao, J., Zhu, Z., Kecskeméthy, A.: Integrated mechanism design and control for completely restrained hybrid-driven based cable paral-

lel manipulators. Journal of Intelligent & Robotic Systems **74**(3-4), 643–661 (2014)
12. Artoni, A.: A methodology for simulation-based, multiobjective gear design optimization. Mechanism and Machine Theory **133**, 95–111 (2019)
13. Cramer, E.J., Dennis Jr, J.E., Frank, P.D., Lewis, R.M., Shubin, G.R.: Problem formulation for multidisciplinary optimization. SIAM Journal on Optimization **4**(4), 754–776 (1994)
14. Balling, R.J., Sobieszczanski-Sobieski, J.: Optimization of coupled systems-a critical overview of approaches. AIAA journal **34**(1), 6–17 (1996)
15. Braun, R., Gage, P., Kroo, I., Sobieski, I.: Implementation and performance issues in collaborative optimization. In: 6th Symposium on Multidisciplinary Analysis and Optimization, p. 4017 (1996)
16. Manning, V.M.: Large-scale design of supersonic aircraft via collaborative optimization (1999)
17. Dunning, P.D., Brampton, C.J., Kim, H.A.: Multidisciplinary level set topology optimization of the internal structure of an aircraft wing. In: 10th World Congress on Structural and Multidisciplinary Optimization, pp. 19–24 (2013)
18. Raymer, D.: Enhancing aircraft conceptual design using multidisciplinary optimization. Ph.D. thesis, Institutionen för flygteknik (2002)
19. Leifsson, L., Ko, A., Mason, W.H., Schetz, J.A., Grossman, B., Haftka, R.T.: Multidisciplinary design optimization of blended-wing-body transport aircraft with distributed propulsion. Aerospace Science and Technology **25**(1), 16–28 (2013)
20. Alonso, J.J., Colonno, M.R.: Multidisciplinary optimization with applications to sonic-boom minimization. Annual Review of Fluid Mechanics **44**, 505–526 (2012)
21. Antoine, N.E., Kroo, I.M.: Framework for aircraft conceptual design and environmental performance studies. AIAA journal **43**(10), 2100–2109 (2005)
22. Ganguli, R., Rajagopal, S.: Multidisciplinary design optimization of an uav wing using kriging based multi-objective genetic algorithm. In: 50th AIAA/ASME/ASCE/AHS/ASC Structures, Structural Dynamics, and Materials Conference 17th AIAA/ASME/AHS Adaptive Structures Conference 11th AIAA No, p. 2219 (2009)
23. Batill, S.M., Stelmack, M.A., Yu, X.Q.: Multidisciplinary design optimization of an electric-powered unmanned air vehicle. Aircraft Design **2**(1), 1–18 (1999)
24. Gu, H., Cai, X., Zhou, J., Li, Z., Shen, S., Zhang, F.: A coordinate descent method for multidisciplinary design optimization of electric-powered winged uavs. In: 2018 International Conference on Unmanned Aircraft Systems (ICUAS), pp. 1189–1198. IEEE (2018)
25. Stengel, R.F.: Flight dynamics. Princeton University Press (2015)
26. Zhang, X., et al.: Aircraft Design Manual Volume VI: Aerodynamic design. China Aviation Publishing & Media (2002)
27. Anderson, J.D.: Aircraft performance and design. McGraw-Hill Science/Engineering/Math (1999)
28. Drela, M.: Xfoil: An analysis and design system for low reynolds number airfoils. In: Low Reynolds number aerodynamics, pp. 1–12. Springer (1989)
29. Gur, O., Mason, W.H., Schetz, J.A.: Full-configuration drag estimation. Journal of Aircraft **47**(4), 1356–1367 (2010)

30. Pennycuick, C.: Mechanics of flight. In: Avian Biology, Volume V, pp. 1–75. Elsevier (1975)
31. Paterson, J., MacWilkinson, D., Blackerby, W.: A survey of drag prediction techniques applicable to subsonic and transonic aircraft design. AGARD Aerodyn. Drag 38 p(SEE N 74-14709 06-01) (1973)
32. Mason, W.: Boundary layer analysis methods. Aerodynamic Calculation Methods for Programmable Calculators & Personal Computers (1981)
33. Shevell, R.S.: Fundamentals of flight (1989)
34. Torenbeek, E.: Synthesis of subsonic airplane design. Delft: Springer (1982)
35. Blackwell Jr, J.A.: Numerical method to calculate the induced drag or optimum loading for arbitrary non-planar aircraft (1976)
36. Falkner, V.: The solution of lifting-plane problems by vortex-lattice theory. Ministry of Supply, Aeronautical Research Council (1947)
37. Prandtl, L.: Tragflügeltheorie. i. mitteilung. Nachrichten von der Gesellschaft der Wissenschaften zu Göttingen, Mathematisch-Physikalische Klasse **1918**, 451–477 (1918)
38. Finck, R., (US), A.F.F.D.L., Hoak, D.: USAF stability and control DATCOM. Engineering Documents (1978)
39. Lyu, X., Gu, H., Wang, Y., Li, Z., Shen, S., Zhang, F.: Design and implementation of a quadrotor tail-sitter vtol uav. In: Robotics and Automation (ICRA), 2017 IEEE International Conference on, pp. 3924–3930. IEEE (2017)
40. Zhang, F., Lyu, X., Wang, Y., Gu, H., Li, Z.: Modeling and flight control simulation of a quadrotor tailsitter vtol uav. In: AIAA Modeling and Simulation Technologies Conference, p. 1561 (2017)
41. Brandt, J., Selig, M.: Propeller performance data at low reynolds numbers. In: 49th AIAA Aerospace Sciences Meeting including the New Horizons Forum and Aerospace Exposition, p. 1255 (2011)
42. John B, B., Robert W, D., Gavin K, A., Michael S, S.: Apc propeller. `http://m-selig.ae.illinois.edu/props/propDB.html` (1999)
43. Traub, L.: Validation of endurance estimates for battery powered uavs. The Aeronautical Journal **117**(1197), 1155–1166 (2013)
44. Kannan, R., Monma, C.L.: On the computational complexity of integer programming problems. In: Optimization and Operations Research, pp. 161–172. Springer (1978)
45. Powell, M.J.: A fast algorithm for nonlinearly constrained optimization calculations. In: Numerical analysis, pp. 144–157. Springer (1978)
46. Byrd, R.H., Gilbert, J.C., Nocedal, J.: A trust region method based on interior point techniques for nonlinear programming. Mathematical Programming **89**(1), 149–185 (2000)
47. Wright, S.J.: Coordinate descent algorithms. Mathematical Programming **151**(1), 3–34 (2015)
48. Grippo, L., Sciandrone, M.: On the convergence of the block nonlinear gauss–seidel method under convex constraints. Operations research letters **26**(3), 127–136 (2000)
49. Saeed, A.S., Younes, A.B., Islam, S., Dias, J., Seneviratne, L., Cai, G.: A review on the platform design, dynamic modeling and control of hybrid uavs. In: Unmanned Aircraft Systems (ICUAS), 2015 International Conference on, pp. 806–815. IEEE (2015)